Enhancement of nonlinear processes near rough nanometer-structured surfaces obtained by deposition of fractal colloidal silver aggregates on a plain substrate

Eugene Poliakov, Vladimir M. Shalaev, and Vladimir Shubin
Department of Physics, New Mexico State University, Las Cruces, New Mexico 88003

Vadim A. Markel
Department of Physics and Astronomy, University of Georgia, Athens, Georgia 30602
(Received 28 April 1999)

In this paper we extend our previous results concerning the enhancement of nonlinear optical responses near rough self-affine metal surfaces to different objects in a wider spectral range and also beyond the quasistatic limit. In our previous work [E. Poliakov *et al.*, Phys. Rev. B **57**, 14 901 (1998)] we studied local and averaged enhancement factors for the second- and third-harmonic generation and degenerate four-wave mixing for nonlinear molecules adsorbed on nanostructured self-affine metal surfaces in the quasistatic approximation in the spectral range from 0.4 to 1.8 μm. In the present work, we study the same nonlinear effects for surfaces formed by deposition on a plane substrate of fractal clusters rather than individual nanoparticles. The spectral range is extended to 10 μm. We have calculated the enhancement factors for the above nonlinear process with the account of retardation and performed numerical calculations for significantly larger samples. Our numerical results indicate that the enhancement factors increase with the wavelength up to $\lambda = 10$ μm. The enhancement of the degenerate four-wave mixing can reach, for example, the value of 10^{22} in the far-infrared spectral region (the maximum enhancement reported by us earlier for this process was $\sim 10^{16}$ near $\lambda = 1.8$ μm). [S0163-1829(99)10539-3]

The optical properties of rough nanometer-structured metallic surfaces (RNSMS) with fractal geometry recently attracted a lot of attention.[1–6] The strong enhancement of local electromagnetic (EM) fields near RNSMS in a wide spectral range can lead to the possibility of performing linear and nonlinear spectroscopic measurements of single molecules adsorbed on a RNSMS.[4,5] The collective nature of the EM energy localization (as opposed to the ''single-scattering'' regime of localization near sharp needles, etc.) provides that the enhancement can take place in a wide spectral region, not just at a particular resonance frequency. It turns out that for any wavelength from ~ 0.5 μm to at least ~ 10 μm, the fractal RNSMS possesses several collective resonant modes (surface modes). Typically, for each frequency, some of the resonant modes are localized and some are delocalized. This chaotic behavior of the localization length was referred to as inhomogeneous localization.[7,8] But, on average, the localization length of the modes that *are localized* tends to decrease with the wavelength λ.[6,9] In addition, the quality factor of the resonances increases with λ in most metals, as a consequence of the Drude formula, up to the maximum wavelength $\lambda_m = 2\pi/\gamma$, where γ is the Drude relaxation constant. Therefore, as λ approaches λ_m, the EM field near a RNSMS becomes localized in hot spots of progressively smaller size and higher intensity. The locations of these ''hot spots'' are wavelength dependent, contrary to what one would expect in the single-scattering regime.

If there is nonlinearity of the host metal, or in molecules adsorbed on the surface, the existence of these zones of high intensity EM fields leads to enhancement of local and average nonlinear optical responses, as was predicted theoretically[10–15] and observed experimentally.[16–21] In our recent numerical calculations,[22] we used experimental optical constants of silver in the range of $\lambda = 0.2$–1.8 μm to estimate the values of the enhancement factors for different nonlinear processes. Our results have indicated that the enhancement of a nonlinear signal can reach the values of 10^7 and 10^{15} for the second- and third-order process, respectively, near $\lambda = 1.8$ μm. However, the value of λ_m is, typically, much larger (for example, $\lambda_m \sim 70$ μm for silver). This prompts that even larger enhancements can be reached when λ approaches λ_m. It is known that the dielectric function of good conductors, such as silver, are well described by the Drude formula in the region $\lambda \gg \lambda_p$, where $\lambda_p = 2\pi c/\omega_p$ and ω_p is the plasmon frequency, and, in particular, in the spectral region where experimental constants of metals are not usually measured. In this paper, we report the results of numerical calculations for λ's up to 10 μm.

In our previous paper,[22] we performed calculations for samples generated in the so-called restricted solid-on-solid model. In this model one assumes that single metal nanoparticles are deposited on a plain substrate from a solution. Here we use an alternative model in which the individual nanoparticles are allowed first to aggregate in the solution and form fractal clusters (cluster-cluster aggregates with the fractal dimension $D \approx 1.8$) and only later are deposited on the substrate. An image of a rough surface formed by this deposition process is shown in Ref. 3. We also used larger clusters with $N = 5000$ elementary units (compared to $N \sim 1000$ in the previous work[22]). Each elementary unit is considered to be a sphere of the size ~ 8 nm, and the characteristic lateral dimension of the samples used in the present work is 1 μm and the maximum vertical height about 120 nm. The results presented here are averaged over four random samples. Note that unlike the self-affine films obtained in the restricted

solid-on-solid model, the samples studied here are characterized by the appearance of ''holes'' or empty spaces of different sizes (see the image in Ref. 3). Such samples more closely resemble the experimental surfaces that were studied recently using the near-field microscopy[1–3,6] and (SERS).[4,5]

To obtain the optical properties, we used the coupled-dipole method[12] with intersections of the neighboring spheres.[9,23] But contrary to our previous work, we did not restrict the dipole-dipole interaction to the quasistatic limit and we used fully retarded dipole fields.

The coupled-dipole equations that couple the linear and nonlinear dipole moments $\mathbf{d}_i(\omega)$ and $\mathbf{d}_i^{NL}(\omega_g)$ of the ith monomer to the incident wave have the form (see Refs. 12 and 22 for more detail)

$$\mathbf{d}_i(\omega)=\alpha(\omega)\left[\mathbf{E}_i^{(0)}+\sum\ \hat{W}_{ij}(\omega)\mathbf{d}_j(\omega)\right], \tag{1}$$

$$\mathbf{d}_i^{NL}(\omega_g)=\alpha(\omega_g)\left[\mathbf{F}_i+\sum\ \hat{W}_{ij}(\omega_g)\mathbf{d}_j^{NL}(\omega)\right]. \tag{2}$$

where ω and ω_g are the frequencies of the linear and generated signals, $\mathbf{E}_i^{(0)}=\mathbf{E}^{(0)}\exp(i\mathbf{k}\cdot\mathbf{r}_i)$ is the amplitude of the incident plane wave at the location of the ith monomer, $\alpha(\omega)$ is the frequency-dependent polarizability of a monomer, $\hat{W}_{ij}(\omega)$ is the fully retarded dipole radiation field produced by a dipole at the jth site oscillating with the frequency ω at the ith site, and $\mathbf{F}_i$ is described below. We calculated $\alpha(\omega)$ using the Lorenz-Lorentz formula with the radiative correction introduced by Draine[24] and with the use of the model of intersecting nearest-neighbor nanoparticles.[9,23] The dielectric function of silver was obtained from the Drude formula $\epsilon(\omega)=\epsilon_0-\omega_p^2/\omega(\omega+i\gamma)$ with the following parameters for silver: $\epsilon_0=5$, $\lambda_p=2\pi c/\omega_p=136$ nm, and $\gamma/\omega_p=0.002$.

The generated signal frequency ω_g and the free term for the equation coupling the nonlinear dipoles to each other, $\mathbf{F}_i$, depend on the specific nonlinear process. In general, $\mathbf{F}_i$ can be expressed in terms of the linear dipole moments $\mathbf{d}_i(\omega)$ or corresponding local electric fields $\mathbf{E}_i(\omega)=\alpha^{-1}(\omega)\mathbf{d}_i(\omega)$. For the processes considered below,

$$\omega_g=2\omega,\quad \mathbf{F}_i=a(\mathbf{E}_i\cdot\mathbf{E}_i)\mathbf{n}_i+b(\mathbf{n}_i\cdot\mathbf{E}_i)\mathbf{E}_i+c(\mathbf{E}_i\cdot\mathbf{n}_i)^2\mathbf{n}_i$$

(second-harmonic generation), (3)

$$\omega_g=3\omega,\quad \mathbf{F}_i=a(\mathbf{E}_i\cdot\mathbf{E}_i)\mathbf{E}_i\ \text{(third-harmonic generation)}, \tag{4}$$

$$\omega_g=\omega,\quad \mathbf{F}_i=a(\mathbf{E}_i\cdot\mathbf{E}_i^*)\mathbf{E}_i+b(\mathbf{E}_i\cdot\mathbf{E}_i)\mathbf{E}_i^*$$

(degenerate four-wave mixing). (5)

Here a,b,c are constants related to nonlinear susceptibilities, probably different for different processes, and $\mathbf{n}_i$'s are the ''preferred direction'' vectors for nonlinear molecules that break the spherical symmetry in order to make the second-harmonic generation possible. For simplicity, we assume below that all the adsorbed molecules have the same ''preferred direction,'' $\mathbf{n}_i=\mathbf{n}$ which is perpendicular to the surface plane.

The physical meaning of Eqs. (1) and (2) is transparent. The first equation couples the linear dipole moments to each other and to the incident wave. The local fields at the incident frequency ω induce nonlinear dipole moments that oscillate at the generated frequency ω_g and are further coupled to each other via dipole radiation fields by Eq. (2). The term $\mathbf{F}_i$ plays the role of the incident field for the nonlinear dipoles and is oscillating at the generated frequency ω_g. Note that in the case of a degenerate nonlinear process (5), both linear and nonlinear dipoles interact at the same frequency and the coupling constants in both Eqs. (1) and (2) are the same: $\alpha(\omega)=\alpha(\omega_g)$; therefore the interaction of nonlinear dipoles cannot be disregarded in the spectral region where the interaction of linear dipoles is known to be strong.

In the numerical simulations the samples were considered to be placed on a surface of a dielectric prism and irradiated by an evanescent incident wave due to the total internal reflection of the incident laser beam from the inner surface of the prism. This setup is the same as in several near-field optical microscopy experiments that detected the existence and spectral dependence of the regions of EM energy localization.[1–3,6] Correspondingly, the incident wave has the form

$$\mathbf{E}_i^{(0)}=\mathbf{E}_0\exp\left[\frac{\omega}{c}(-z\sqrt{n^2\sin^2\theta-1}+ixn\sin\theta)\right], \tag{6}$$

where θ is the angle of incidence for the laser beam (set to $\pi/4$ in the calculations) and $n=1.58$ is the refractive index of the prism, the z axis is perpendicular to the prism surface and the x axis is parallel to the propagation direction of the evanescent wave.

One of the possible definitions for the nonlinear enhancement factor utilizes the idea of work that would be done by a weak probe field oscillating at the *generated* frequency ω_g on the nonlinear dipoles. This definition is convenient because it allows one to express the enhancement factors in terms of linear local fields only. The general formula for an enhancement factor G is[22]

$$G=\left|\frac{\left\langle\sum_i \mathbf{d}_i^{NL}(\omega_g)\cdot\mathbf{E}_i^{(0)*}(\omega_g)\right\rangle_{\text{on the surface}}}{\left\langle\sum_i \mathbf{d}_i^{NL}(\omega_g)\cdot\mathbf{E}_i^{(0)*}(\omega_g)\right\rangle_{\text{in dilute solution}}}\right|^2. \tag{7}$$

There are few conventions adopted in the above definition. First, $\mathbf{E}_i^{(0)}(\omega_g)=\mathbf{E}^{(0)}\exp(i\mathbf{k}_g\cdot\mathbf{r}_i)$ is the amplitude of the *probe* field which is oscillating at the generated frequency ω_g rather than the incident frequency ω. It can be obtained from Eq. (6) by replacing ω by ω_g. The summation Σ_i is over all possible locations of nonlinear molecules on the outer surface of the sample. The term in the numerator of Eq. (7) is calculated when the molecules are placed on the surface of a RNSMS and the denominator—when the same molecules are in a dilute solution and are irradiated only by the incident wave [Eq. (6)]. Finally, the averaging $\langle\cdots\rangle$ is over random sample realizations. Note that both the numera-

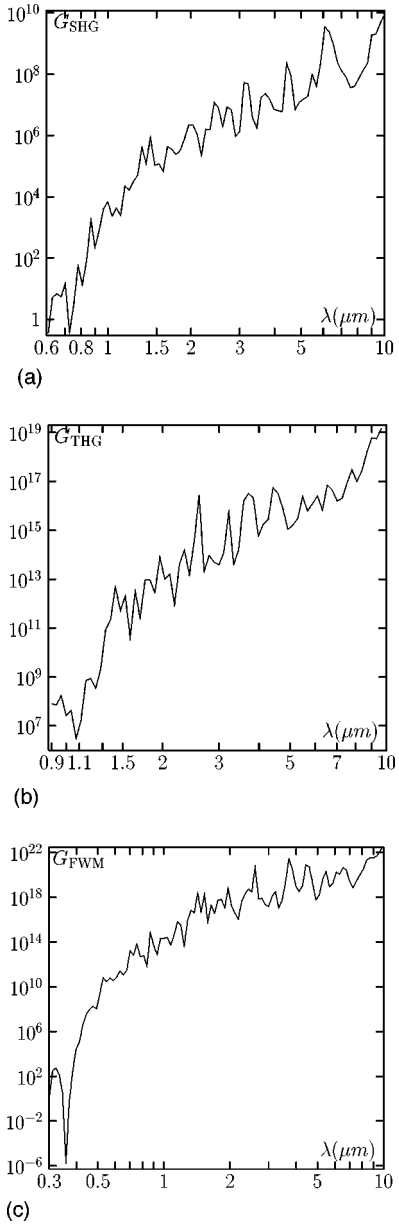

FIG. 1. Average enhancement factors for the second-harmonic generation (a), third-harmonic generation (b), and degenerate four-wave mixing (c) as functions of the wavelength.

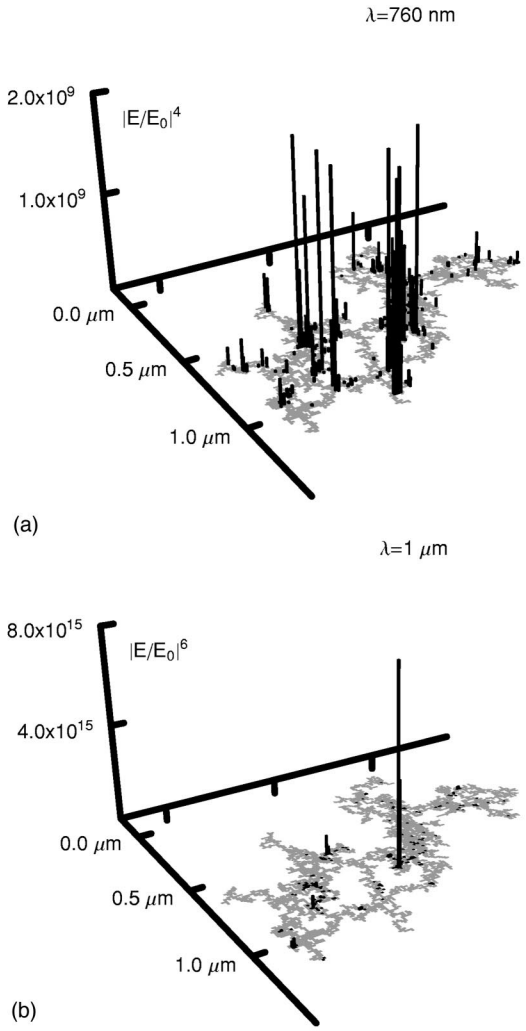

FIG. 2. Distribution of the local enhancement factors at the surface of a computer-generated sample for the second-harmonic generation at the wavelength of the incident linear wave $\lambda = 760$ nm (a) and for the third-harmonic generation at $\lambda = 1$ μm (b). The generated signal wavelength is close to 300 nm in both cases. It is assumed that the nonlinear moments at the generated frequency are not coupled.

tor and the denominator in Eq. (7) are bilinear in dipole moments or local electric fields, as would be expected for an enhancement factor. The amplitudes of the probe field are independent of the solution to the coupled-dipole equations.

Although the definition (7) utilizes the amplitudes of nonlinear dipole moments that must be calculated from Eq. (2) after Eq. (1) is solved to determine the appropriate free terms $\mathbf{F}_i$, the similar structure of Eqs. (1) and (2) allows one to express G in terms of linear dipole moments only. Using the fact that the solutions to Eqs. (1) and (2) can be written in the form $\mathbf{d}_i(\omega) = \Sigma_j \hat{\kappa}_{ij} \mathbf{E}_j^{(0)}$ and $\mathbf{d}_i^{NL}(\omega_g) = \Sigma_j \hat{\kappa}_{ij} \mathbf{F}_j$, where $\hat{\kappa}_{ij}$ is a symmetrical tensor such that $(\hat{\kappa}_{ij})_{\alpha\beta} = (\hat{\kappa}_{ji})_{\beta\alpha}$, it is possible to show that $\Sigma_i \mathbf{d}_i^{NL}(\omega_g) \cdot \mathbf{E}_i^{(0)*}(\omega_g) = \Sigma_i \mathbf{F}_i \cdot \mathbf{d}_i^{+}(\omega_g)$, where $\mathbf{d}_i^{+}(\omega_g)$ is the solution to the equation obtained from Eq. (1) by taking the complex conjugate of the free term $\mathbf{E}_i^{(0)}$, i.e., for the incident evanescent wave propagating in the negative x direction. Consequently, formula (7) can be rewritten as

$$G = \left| \frac{\left\langle \sum_i \mathbf{F}_i \cdot \mathbf{E}_i^{+}(\omega_g) \right\rangle_{\text{on the surface}}}{\left\langle \sum_i \mathbf{F}_i^{(0)} \cdot \mathbf{E}_i^{(0)*}(\omega_g) \right\rangle_{\text{in dilute solution}}} \right|^2, \qquad (8)$$

where $\mathbf{F}_i$ is related to the linear local fields $\mathbf{E}_i$ by one of Eqs. (3)–(5), $\mathbf{E}_i^{+}(\omega_g) = \alpha^{-1}(\omega_g) \mathbf{d}_i^{+}(\omega_g)$, and $\mathbf{F}_i^{(0)}$ is determined from the same equations with the local fields substituted by the incident fields $\mathbf{E}_i^{(0)}$.

Now we turn to the results of calculations which are shown in Figs. 1 and 2. Figure 1 illustrates the wavelength dependence of the averaged enhancement factor G for the second- and third-harmonic generation and the degenerate

four-wave mixing. Apart from random fluctuations which are associated with numerical averaging and are not expected to be seen experimentally, the general trend is the increase of enhancement with the wavelength. Note that the spectral ranges for different nonlinear processes differ in Figs. 1(a)–1(c). This is explained by the fact that according to Eq. (8), to determine the enhancement factor at a specific incident wavelength λ one needs also to find linear responses at the generated wavelength λ_g. For the second- and third-harmonic generation, λ_g is two and three times, respectively, smaller than λ. On the other hand, the Drude formula used in this work to calculate $\alpha(\lambda)$ is accurate only for $\lambda > 300$ nm. Therefore the data for the second-harmonic generation start from $\lambda = 600$ nm and for the third-harmonic generation from $\lambda = 900$ nm (λ_g is in both cases equal to 300 nm which corresponds to the lower bound of the spectrum).

As one could expect, the enhancement is larger for the third-order nonlinear processes [Figs. 1(b) and 1(c)] than for the second order [Fig. 1(a)]. This happens because for the higher-order nonlinearities the local fields in Eqs. (3)–(5) are raised to a greater power. Further, the enhancement is larger for the degenerate four-wave mixing than for the third-harmonic generation, although both are third-order nonlinear processes. This can be understood by examining Eqs. (1) and (2). In the case of a degenerate process, $\omega = \omega_g$ and the linear local fields are first enhanced by Eq. (1) and then the nonlinear fields are enhanced by Eq. (2) at the same frequency. But for the third-order harmonic generation, the coupling of nonlinear fields occurs at the tripled frequency $\omega_g = 3\omega$, when both the resonance quality factor and localization are significantly smaller. We obtained the maximum enhancement for the degenerate four-wave mixing near $\lambda = 10\ \mu$m of 10^{22}.

Finally, in Fig. 2 we present the distribution of local fields on the surface raised to the fourth [Fig. 2(a)] and sixth [Fig. 2(b)] powers, at $\lambda = 760$ nm and 1 μm, respectively, which roughly corresponds to the local enhancement of the second- and the third-harmonic generation when the coupling of *nonlinear* dipoles via Eq. (2) can be neglected. In both cases the generated wavelength is close to 330 nm (the surface-plasmon resonance wavelength) when the coupling is known to be small.[9,12] By comparing Figs. 1(a) and 2(a), we see that while the average enhancement of the second-harmonic generation is close to unity at $\lambda = 760$ nm, the maximum *local* enhancement can reach 10^9. It can be probed by placing a single molecule in the surface region where the EM energy is highly concentrated at a given wavelength. As was shown in Ref. 6, the locations of such hot spots are extremely wavelength and polarization sensitive and can span large portions of the surface in a relatively small spectral range. A comparison of corresponding figures for the third-harmonic generation [Figs. 1(b) and 2(b)] shows again that the maximum local enhancement can be 8–9 orders of magnitudes higher than the averaged value. This allows us to predict extremely high local enhancements of nonlinear signals in the far-infrared region of the spectrum considered in this paper (near $\lambda = 10\ \mu$m).

This research was supported by NSF Grant No. DMR-9810183. The computational facilities were provided by the National Center for Supercomputing Applications under Grant No. PHY980006N.

[1] S. I. Bozhevolnyi, B. Vohnsen, A. V. Zayats, and I. I. Smolyaninov, Surf. Sci. **356**, 268 (1996).
[2] S. I. Bozhevolnyi, Phys. Rev. B **54**, 8177 (1996).
[3] S. I. Bozhevolnyi, V. A. Markel, V. Coello, W. Kim, and V. M. Shalaev, Phys. Rev. B **58**, 11 441 (1998).
[4] K. Kneipp, H. Kneipp, V. B. Kartha, R. Manoharan, G. Deinum, I. Itzkan, R. R. Dasari, and M. S. Feld, Phys. Rev. E **57**, R6281 (1998).
[5] K. Kneipp, H. Kneipp, V. B. Kartha, R. Manoharan, G. Deinum, I. Itzkan, R. R. Dasari, and M. S. Feld, Appl. Spectrosc. **52**, 1493 (1998).
[6] V. A. Markel, V. M. Shalaev, P. Zhang, W. Huyanh, L. Tay, T. L. Haslett, and M. Moskovits, Phys. Rev. B **59**, 10 903 (1999).
[7] M. I. Stockman, Phys. Rev. E **56**, 6494 (1997).
[8] M. I. Stockman, Phys. Rev. Lett. **79**, 4562 (1997).
[9] V. A. Markel, V. M. Shalaev, E. B. Stechel, W. Kim, and R. L. Armstrong, Phys. Rev. B **53**, 2425 (1996).
[10] V. M. Shalaev and M. I. Stockman, Zh. Éksp. Teor. Fiz. **92**, 509 (1987) [Sov. Phys. JETP **65**, 287 (1987)].
[11] A. V. Butenko, V. M. Shalaev, and M. I. Stockman, Zh. Éksp. Teor. Fiz. **94**, 107 (1988) [Sov. Phys. JETP **67**, 60 (1988)].
[12] V. A. Markel, L. S. Muratov, M. I. Stockman, and T. F. George, Phys. Rev. B **43**, 8183 (1991).
[13] V. M. Shalaev, M. I. Stockman, and R. Botet, Physica A **185**, 181 (1992).
[14] M. I. Stockman, V. M. Shalaev, M. Moskovits, R. Botet, and T. F. George, Phys. Rev. B **46**, 2821 (1992).
[15] V. M. Shalaev, E. Y. Poliakov, and V. A. Markel, Phys. Rev. B **53**, 2437 (1996).
[16] S. G. Rautian, V. P. Safonov, P. A. Chubakov, V. M. Shalaev, and M. I. Stockman, Pis'ma Zh. Éksp. Teor. Fiz. **47**, 200 (1988) [JETP Lett. **47**, 243 (1988)].
[17] A. V. Butenko, P. A. Chubakov, Y. E. Danilova, S. V. Karpov, A. K. Popov, S. G. Rautian, V. P. Safonov, V. V. Slabko, V. M. Shalaev, and M. I. Stockman, Z. Phys. D **17**, 283 (1990).
[18] Y. E. Danilova, S. G. Rautian, and V. P. Safonov, Bull. Russian Acad. Sci. Phys. **60**, 374 (1996).
[19] Y. E. Danilova, V. P. Drachev, S. V. Perminov, and V. P. Safonov, Bull. Russian Acad. Sci. Phys. **60**, 342 (1996).
[20] Y. E. Danilova, N. N. Lepeshkin, S. G. Rautian, and V. P. Safonov, Physica A **241**, 231 (1997).
[21] V. P. Drachev, S. V. Perminov, S. G. Rautian, and V. P. Safonov, Pis'ma Zh. Éksp. Teor. Fiz. **68**, 618 (1998) [JETP Lett. **68**, 651 (1998)].
[22] E. Y. Poliakov, V. A. Markel, V. M. Shalaev, and R. Botet, Phys. Rev. B **57**, 14 901 (1998).
[23] V. A. Markel and V. M. Shalaev, in *Computational Studies of New Materials*, edited by D. A. Jelski and T. F. George (World Scientific, Singapore, 1999), pp. 210–243.
[24] B. T. Draine, Astrophys. J. **333**, 848 (1988).